Phonon Raman scattering of $R\mathrm{CrO_3}$ perovskites (R = Y, La, Pr, Sm, Gd, Dy, Ho, Yb, Lu)

M. C. Weber,[1] J. Kreisel,[1,2,*] P. A. Thomas,[1] M. Newton,[1] K. Sardar,[3] and R. I. Walton[3]

[1]*Department of Physics, University of Warwick, Coventry CV4 7AL, United Kingdom*

[2]*Laboratoire Matériaux et Génie Physique, Minatec, CNRS, Grenoble Institute of Technology, 3, parvis Louis Néel, 38016 Grenoble, France*

[3]*Department of Chemistry, University of Warwick, Coventry CV4 7AL, United Kingdom*

(Received 15 December 2011; published 9 February 2012)

We report a systematic investigation of orthorhombic perovskite-type $R\mathrm{CrO_3}$ powder samples by Raman scattering for nine different rare earth R^{3+} cations (R = Y, La, Pr, Sm, Gd, Dy, Ho, Yb, and Lu). The room-temperature Raman spectra and the associated phonon mode assignment provide reference data for structural investigation of the whole series of $R\mathrm{CrO_3}$ orthochromites and phonon *ab-initio* calculations. The assignment of the chromite spectra and comparison with Raman data on other orthorhombic perovskites allows correlating the phonon modes with the structural distortions in the $R\mathrm{CrO_3}$ series. In particular, two A_g modes are identified as octahedra rotation soft modes, as their positions scale linearly with the octahedra tilt angle of the $\mathrm{CrO_6}$ octahedra.

DOI: 10.1103/PhysRevB.85.054303 PACS number(s): 78.30.−j, 63.20.−e

I. INTRODUCTION

The understanding of functional $AB\mathrm{O_3}$ perovskite-type oxides is a very active research area with relevance to both fundamental- and application-related issues. A particular aspect of perovskites is their capacity to adopt a multitude of different structural distortions due to the possible incorporation of almost every element of the periodic table into their structure.[1] Such distortions can be driven by external parameters, like temperature, pressure, or chemical composition, which leads to an extraordinary richness of physical properties within the family of perovskites. Multiferroic perovskites, which possess simultaneously several so-called ferroic orders, such as ferromagnetism, ferroelectricity, and/or ferroelasticity, currently attract specific interest.[2–4] Structural distortions in perovskites can be described by separating three main features with respect to their ideal cubic structure:[1,5,6] (i) a rotation (tilt) of essentially rigid $B\mathrm{O_6}$ octahedra, (ii) polar cation displacements, which often lead to ferroelectricity, and (iii) distortions of the octahedra, such as the Jahn–Teller distortion. Past investigations of these instabilities have been a rich source for the understanding of structural properties, not only in perovskites, but also in oxides in general. The most common distortion in perovskites is the tilt of octahedra. Although many different octahedral tilt systems exist,[1,5–7] the R-3c structure with tilt system $a^-a^-a^-$ (Glazer's notation[6]) and the *Pnma* with $a^-b^+a^-$ are by far the most common structures found in perovskites.

We are particularly interested in perovskites with the orthorhombic *Pnma* structure, which is, for instance, adopted by $R\mathrm{FeO_3}$ orthoferrites, $R\mathrm{MnO_3}$ orthomanganites, $R\mathrm{NiO_3}$ orthonickelates, or $R\mathrm{ScO_3}$ orthoscandates (R = rare earth). In all these perovskites, the orthorhombic distortion (octahedral tilt angle) can be continuously tuned by the ionic size r_R of the R^{3+} rare earth. This rotation is equivalent to modify the B-O-B bond angle and the B-O orbital overlap, which in turn leads to a rich magnetic phase diagram for magnetic B cations, accompanied by intriguing metal insulator phase transitions when B = Mn and Ni. In this paper, we focus on the family of $R\mathrm{CrO_3}$ orthochromites, which have in the past attracted considerable interest for their complex magnetic phases at low temperature[8–11] and, more recently, for their potential magnetoelectric or multiferroic properties,[11–15] similar to manganites and nickelates.

The aim of our paper is to provide a better understanding of the phonon spectra of $R\mathrm{CrO_3}$ and to correlate individual phonon modes to the structural distortions of the structure. For this, we have investigated $R\mathrm{CrO_3}$ powder samples with a large number of different rare earth (Y, La, Pr, Sm, Gd, Dy, Ho, Yb, and Lu) by phonon Raman spectroscopy, which is known to be a versatile technique for the investigation of both phase transitions[16–23] and more subtle structural distortions in perovskites.[24–29] While the Raman signature of orthomanganites[24–27,30,31] or orthoferrites[32–34] is well known and understood, investigations of orthochromites remain limited to Raman studies for R = Y, La, Nd, Gd, Ho, and Er,[22,24,35–38] out of which the single-crystal work on $\mathrm{LaCrO_3}$ (Ref. 22) and $\mathrm{YCrO_3}$ (Ref. 24) is of particular relevance for this paper. However, the whole $R\mathrm{CrO_3}$ series has not yet been systematically investigated.

II. EXPERIMENTAL

Powder samples of $R\mathrm{CrO_3}$ (R = Y, La, Pr, Sm, Gd, Dy, Ho, Yb, and Lu) chromites were synthesized by a direct hydrothermal synthesis that gave polycrystalline powders of a greenish color. More details about the synthesis of samples can be found in Ref. 10. The high quality of the samples has been attested by previous x-ray diffraction measurements and the characterization of their magnetic properties.[10] Throughout this paper, we will discuss the different structural details of orthochromites; Table I presents a resume of these characteristics for both the chromites investigated here and others discussed in the text. Particular attention has been paid to the calculation of the octahedral tilt angles. This is not straightforward for the *Pnma* structure, as the angles can be calculated either from cell parameters or from the atomic coordinates;[1] both results are compared in Table I. Typically, the use of cell parameters introduces an error in the tilt angles by about 3°, sometimes even more, as the octahedra are slightly distorted, and we thus rather rely on the tilt angles which we have calculated from the atomic coordinates according to the

TABLE I. Structural characteristics of RCrO$_3$ samples: lattice parameters in the orthorhombic setting, R^{3+} ionic radii (r_{R3+} values given in an eightfold environment from Ref. 40) and octahedral tilt angles (ϕ[010], θ[101]). The tilt angles are determined both from lattice parameters (Ref. 1) and, where available, from atomic coordinates (Ref. 39). The lattice parameters for NdCrO$_3$ are taken from Ref. 38, for ErCrO$_3$ from Ref. 41, and for all other chromites from Ref. 10. The atomic positions for the calculation of tilt angles are taken from Refs. 41–45.

							CrO$_6$ octahedra tilt angles			
							From lattice parameters		From atomic positions	
	Lattice parameters									
	r_{R3+} (Å)	a (Å)	b (Å)	c (Å)	V (Å^3)	t	$\phi_{[010]}$ (°)	$\theta_{[101]}$ (°)	$\phi_{[010]}$ (°)	$\theta_{[101]}$ (°)
LaCrO$_3$	1.160	5.494	7.777	5.520	235.814	0.903	2.50	5.57	5.25	10.92
PrCrO$_3$	1.126	5.473	7.717	5.496	232.104	0.891		5.20		
NdCrO$_3$	1.109	5.480	7.699	5.425	228.800	0.885	4.79	8.12	7.55	13.86
SmCrO$_3$	1.079	5.524	7.637	5.366	226.328	0.874	6.45	13.73		
GdCrO$_3$	1.053	5.529	7.605	5.313	223.395	0.864	8.91	16.06	10.96	14.39
DyCrO$_3$	1.027	5.526	7.547	5.262	219.428	0.855	9.61	17.77	12.09	17.19
YCrO$_3$	1.019	5.520	7.536	5.255	218.606	0.852	9.56	17.85	12.20	16.98
HoCrO$_3$	1.015	5.533	7.534	5.243	218.554	0.851	10.21	18.62		
ErCrO$_3$	1.004	5.503	7.504	5.214	215.303	0.847	10.70	18.66	12.23	17.32
YbCrO$_3$	0.985	5.525	7.497	5.202	215.462	0.840	11.13	19.70		
LuCrO$_3$	0.977	5.524	7.494	5.186	214.667	0.837	11.89	20.16		

formalism and formula in Ref. 39:

$$\theta = \arctan\left[4\frac{\sqrt{w_{O(1)}^2 + u_{O(1)}^2}}{b}\right],$$
$$\varphi = \arctan\left[4\frac{\sqrt{w_{O(2)}^2 + u_{O(2)}^2}}{\sqrt{c^2 + a^2}}\right]. \quad (1)$$

In order to illustrate the distortion throughout the series, Fig. 1 presents the evolution of the lattice parameters and the tolerance factor t, defined as $t = (r_{R3+} + r_{O2-})/\sqrt{2}\,(r_{Cr3+} + r_{O2-})$.

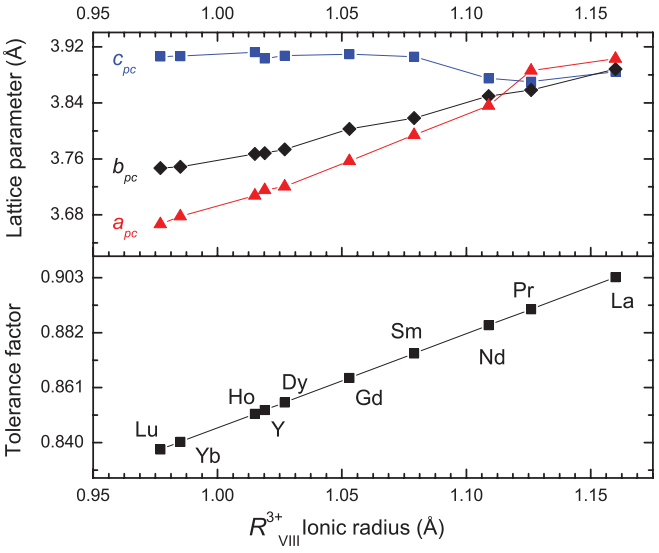

FIG. 1. (Color online) Variation of the pseudocubic cell parameters and the tolerance factor for RCrO$_3$ as a function of the $R^{3+}{}_{VIII}$ ionic radius. The lattice parameters for NdCrO$_3$ are taken from Ref. 38, for all other chromites from Ref. 10.

Raman spectra were recorded with a Renishaw inVia Reflex Raman Microscope with a low wave number spectral cutoff at about 120 cm^{-1}. Experiments were conducted in micro-Raman mode at room temperature by using a 633-nm He-Ne laser as an exciting wavelength. It is well known that Raman spectra recorded on transition-metal oxides, such as orthomanganites[30,46] or orthonickelates,[29,47] often show a strong dependence on the exciting laser power, leading to structural modifications, phase transitions, or even locally decomposed material. Contrary to the above samples, our RCrO$_3$ powders are not black where laser heating is naturally expected. Nevertheless, we have observed that experiments with a laser power above 10 mW lead to a significantly modified spectral signature RCrO$_3$ in terms of band position, width, and intensity due to local laser heating. As a consequence, our experiments have been carried out using laser powers of <1 mW under the microscope, and we have carefully verified that no structural transformations or overheating take place.

III. RESULTS AND DISCUSSION

The ideal cubic structure of ABO_3 perovskites is rather simple, with corner-linked anion octahedra BO_6, the B cations at the center of the octahedra, and the A cations in the space between the octahedra. In this cubic perovskite structure, Raman scattering is forbidden by symmetry.

Here, RCrO$_3$ chromites crystallize in an orthorhombically distorted perovskite structure with space group $Pnma$ (alternative setting $Pbnm$). With respect to the ideal cubic $Pm\bar{3}m$ perovskite structure, this orthorhombic $Pnma$ structure is obtained by an antiphase tilt of the adjacent CrO$_6$ octahedra ($a^-b^+a^-$ in Glazer's notation[6]). The tilting of the CrO$_6$ octahedra necessarily induces a distortion of the RO_{12} polyhedra. In the $Pnma$ structure, the A cation is usually considered to be in eight coordination, and also antiparallel A cation displacements are permitted by symmetry. Here, Cr^{3+} is a Jahn–Teller (JT) inactive cation, leading to almost no dispersion in the Cr-O

TABLE II. Band positions and assignment of the observed Raman modes in RCrO$_3$. While the symmetry assignment is discussed in text, the activating distortions (Ref. 22) and main atomic motions are extended from Refs. 22, 24, and 26.

Symmetry	LuCrO$_3$	YbCrO$_3$	HoCrO$_3$	YCrO$_3$	DyCrO$_3$	GdCrO$_3$	SmCrO$_3$	PrCrO$_3$	LaCrO$_3$	Activating distortion	Main atomic motions
A_g (1)				149.0							
A_g (2)	137.6	138.5	141.2	184.5	141.0	142.2	140.8	143.5	175.2	rot[101]	$A(z)$ out of plane
A_g (3)	285.9	278.0	274.3	281.8	270.2	255.5	231.5	193.2	104.0	rot[010], JT	BO_6 in-phase y rotations
A_g (4)	353.4	351.7	341.3	338.8	335.6	324.9	309.1	279.9	255.3	A shift	$O_1(x)$, $A(-x)$
A_g (5)	446.8	441.7	419.6	421.1	409.5	392.4	365.7	320.9	274.7	rot[101]	BO_6 out-of-phase x rotations
A_g (6)	508.2	501.9	493.3	489.1	486.1	477.0	465.3	449.7	436.6	rot[101]	BO_6 bendings
A_g (7)				558.3		561.2					
B_{1g} (1)	265.6	260.7	260.3	273.1	260.5	245.3	244.7				
B_{1g} (2)	411.8	408.8	401.6	405.4	397.2	388.7	382.4	365.4	351.4	A shift	$A(z)$, $O_1(-z)$
B_{2g} (1)	161.3	161.4	162.1	216.8	160.4	159.3	155.2	149.1	151.7	rot[101]	$A(x)$
B_{2g} (2)	339.8	332.4	315.2	316.7	305.5	284.5	252.7	201.1	124.6	A shift	$A(z)$, $O_1(z)$
B_{2g} (3)	519.2	514.1	493.3	498.3	490.6	473.6	460.9	425.5	405.4	rot[101]	BO_6 out-of-phase bendings
B_{3g} (1)			129.2	171.5	130.5	137.1				rot[101]	$A(y)$
B_{3g} (2)	497.4	504.7	486.9	482.3	482.2	473.6	454.7	443.8	424.5	rot[101]	out-of-phase O_2 scissors-like
B_{3g} (3)	565.1	563.8	562.9	540.5	560.0	568.7	567.2	577.7	586.8	rot[101]	O_2,O_1 antistretching

bonds, typically an order of magnitude lower than what is observed in JT-active orthomanganites. All three distortions (tilt, octahedra distortion, and A-cation displacement) break the cubic symmetry and thus activate zone center Raman modes.[22] According to group theory, the orthorhombic *Pnma* structure with four formula units per unit cell gives rise to 24 Raman-active modes:[30] $7\ A_g + 5\ B_{1g} + 7\ B_{2g} + 5\ B_{3g}$.

Raman spectra of orthochromites with R = La, Pr, Sm, Gd, Dy, Ho, Yb, and Lu are presented in Fig. 2 and show 11 to 14 modes depending on the rare earth. The other predicted modes

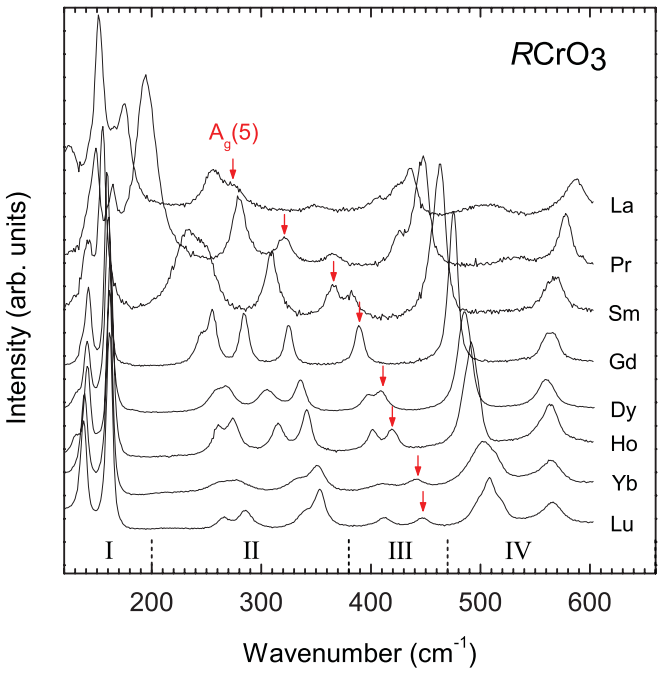

FIG. 2. (Color online) Raman spectra at 300 K of RCrO$_3$ powders (R = La, Pr, Sm, Gd, Dy, Ho,Yb, and Lu) collected with a 632.8-nm He-Ne laser line. I, II, III, and IV denote specific spectral regions discussed in the text. The red/dark gray arrows illustrate for a specific mode, how the phonons can be followed through the series of RCrO$_3$.

are either of too low intensity to be observed or below our experimental cutoff. Our powder Raman spectra of LaCrO$_3$, GdCrO$_3$, and HoCrO$_3$ are consistent with literature work on single crystals of the same materials;[22,24,35,36] for the other five chromites there is to date no data in the literature to the best of our knowledge. Table II presents the position and the hereafter discussed assignment of the individual modes together with their notation used in this paper.

Qualitatively, the overall spectral signature of the chromites is similar, in agreement with their shared space group, where the orthorhombic distortion varies continuously from the smallest rare earth Lu ($r_{\mathrm{Lu,VIII}}$ = 0.98 Å) to the largest rare earth La ($r_{\mathrm{La,VIII}}$ = 1.16 Å).[10,40] According to Fig. 1, LaCrO$_3$ and PrCrO$_3$ occupy a special place in the orthochromite series in the sense that their orthorhombic distortion is significantly smaller than that of other orthochomites with very close lattice parameters a, b, and c. Consistently, the spectra of LaCrO$_3$ and PrCrO$_3$ differ the most from the other spectra of the series, namely in the low and mid wave number range, suggesting that the Raman signature can be used to follow the orthorhombic distortion.

A. Symmetry assignment of Raman modes in RCrO$_3$

A symmetry assignment of the different Raman features is the *sine qua non* condition for a later discussion of the correlation between structural distortions and the Raman signature. Generally speaking, the use of powder samples with a random orientation of crystallites, as in our study, inhibits the assignment of Raman modes by using polarized configurations. As a consequence, the hereafter presented assignment is in a first step based on single crystal measurements that have been reported in the literature for LaCrO$_3$ (Ref. 22), GdCrO$_3$ (Ref. 35), YCrO$_3$ (Refs. 24 and 35), and HoCrO$_3$ (Ref. 36). In a second step, we have taken advantage of the continuous changes in the Raman spectra across the whole RCrO$_3$ series, which has allowed verifying the reported literature assignments, assigning the modes for the not-yet-reported samples and investigating the crossing of several modes. For

the sake of clarity and given the important number of both materials and Raman bands, we will successively discuss four spectral regions as defined in Fig. 2:

(i) Region I (below 200 cm^{-1}) characterized by two sharp and intense bands,

(ii) Region II (200 to 380 cm^{-1}) characterized by four partly overlapping bands,

(iii) Region III (380 to 500 cm^{-1}) with two bands of similar intensity, except for $GdCrO_3$, where only one band is observed, and

(iv) Region IV (500 to 600 cm^{-1}) with two features, each characterized by overlapping bands.

1. Region I (below 200 cm^{-1})

In the approximation of an harmonic oscillator $\omega = (k/\mu)^{1/2}$ (k, force constant; μ, reduced mass), the heaviest atom of the structure is expected to vibrate in the low wave number region. Among the materials shown in Fig. 2, the mass increases only by about 25% from La to Yb, so that the frequency associated with A-cation vibrations is expected to increase only a little with decreasing mass. Bands which are dominated by vibrations of the A cation are expected to be only a little affected by changes in the orthorhombic distortion.

The two sharp low wave number bands at 137 and 161 cm^{-1} (values for $LuCrO_3$) show only small variation despite the large changes in distortion throughout the series. It is thus natural to assign these two bands to A-cation vibrations.

The most convincing argument for the assignment of the two low wave number bands to A-cation vibrations comes from Fig. 3, which compares the Raman spectrum of $YCrO_3$ to that of $DyCrO_3$ and $HoCrO_3$. The three rare earth elements have close ionic radii for Dy ($r_{Dy,VIII} = 1.03$ Å), Y ($r_{Y,VIII} = 1.02$ Å), and Ho ($r_{Ho,VIII} = 1.02$ Å), leading to a very similar orthorhombic distortion, but the mass of the Y ($m_Y = 89$) is very different to that of Dy ($m_{Dy} = 162.5$) and Ho ($m_{Ho} = 165$). It can be seen from Fig. 3 that the sharp bands shift for $YCrO_3$ significantly by about 45 cm^{-1}, while the other bands are only a little or not affected. The inset of Fig. 3 shows that this shift, for the band at 137 cm^{-1}, corresponds well to the mass-induced shift expected from a harmonic oscillator. This observation provides conclusive evidence that the two sharp low wave number modes are largely dominated by vibrations of the A cation. Following the symmetry assignment from single-crystal work on $YCrO_3$,[24] we assign the lower mode to A_g and the higher mode to B_{2g} symmetry. Beyond clarifying the band assignment, it is interesting to note that Fig. 3 illustrates that materials like $YCrO_3$ or $HoCrO_3$, which present an almost identical distortion and thus a rather similar XRD pattern, can be easily differentiated by Raman scattering.

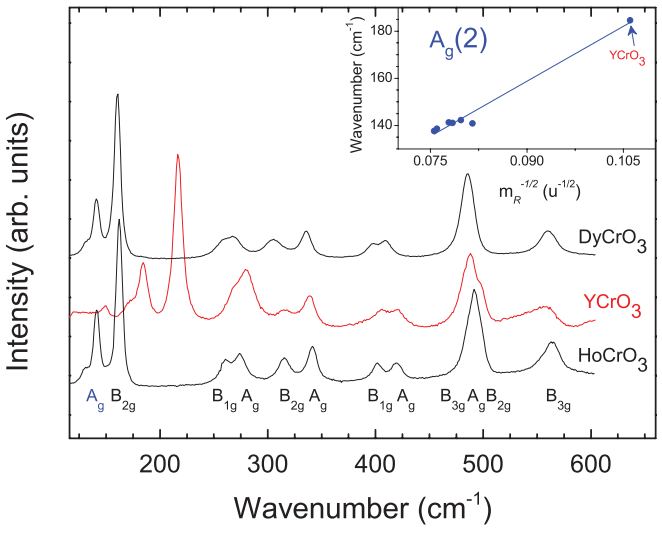

FIG. 3. (Color online) Comparison of Raman spectra for of $HoCrO_3$ (bottom, black), $YCrO_3$ (middle, red/dark gray), and $DyCrO_3$ (top, black) illustrating a significant shift of the low wave number modes for $YCrO_3$. The assignment of A_g, B_{1g}, B_{2g}, and B_{3g} modes is based on Ref. 24 for $YCrO_3$. The inset shows the mass-dependent evolution of the two low wave number bands.

2. Region II (200 to 380 cm^{-1})

Region II is characterized by two doublets, which can be assigned by extension of single-crystal literature data[24,35,36] to bands of B_{1g} symmetry at 265 cm^{-1}, A_g at 285 cm^{-1}, B_{2g} at 339 cm^{-1}, and A_g at 353 cm^{-1} (values for $LuCrO_3$). Different spectral features should be commented upon: (i) Fig. 3 shows that the B_{1g}-A_g doublet around 275 cm^{-1} is affected by changes in the mass of the A cation, while the doublet around 340 cm^{-1} is not. (ii) The B_{2g} mode shows a very significant low wave number shift with increasing radii of the rare earth (decreasing distortion), making its attribution difficult for $LaCrO_3$ and $PrCrO_3$. (iii) As an overall trend, we note that this spectral region is greatly affected by changes in the orthorhombic distortion, which becomes namely obvious for the materials with large r_R (thus reduced orthorhombicity), as will be discussed later.

3. Region III (380 to 500 cm^{-1})

Region III is characterized by two bands of similar intensity; the evolution of their band position across the $RCrO_3$ series is presented in more detail in Fig. 4. For the smallest R^{3+} in $LuCrO_3$, the two bands at 411 and 446 cm^{-1} are well separated and can be assigned to B_{1g} and A_g symmetry, respectively. Due to a pronounced low wave number shift of the A_g (5) band with increasing r_R, the B_{1g} (2) and A_g (5) modes gradually approach until only a single and more intense band is observed for $GdCrO_3$. Upon further increase of r_R, the two modes gradually split again. This continuous evolution of both bands and the observation of a single intense band for $GdCrO_3$ strongly suggest a mode crossing. As the two modes have different B_{1g} and A_g symmetry, such a mode crossing is allowed by symmetry. The low wave number shift of the A_g (5) band throughout the whole series of nine rare earth elements is remarkable and the most pronounced shift observed in the spectra. For the case of $LaCrO_3$, we note that the A_g (5) band has shifted to such an extent that it closely approaches a lower lying A_g (4) mode of region II (see Fig. 2). Such a closeness of modes with the same symmetry can result in a mixing of the modes, as reported in the similar orthomanganites,[26] although we note that the intensity of the modes suggests that a transfer of the character has not yet occurred. The origin of the pronounced shift of the A_g (5) band will be discussed later in more detail.

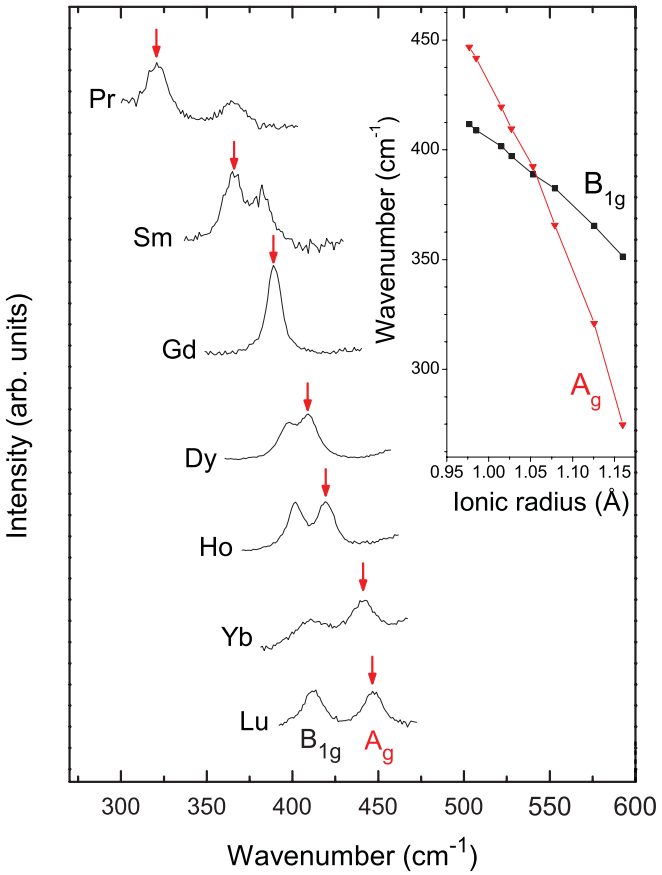

FIG. 4. (Color online) Detailed view of the mid wave number spectral region III. (a) Raman modes and (b) evolution of the band positions with r_R for RCrO$_3$.

4. Region IV (500 to 600 cm^{-1})

Region IV looks at first sight rather simple with only two broad spectral features, but a closer inspection of Fig. 2 shows that it is in fact a rather complex region with an important number of overlapping and crossing bands. The presence of three overlapping features at 497, 508, and 519 cm^{-1} is best observed for the most distorted LuCrO$_3$ and can be assigned to B_{3g}, A_g, and B_{2g} symmetry, respectively. The different symmetries allow these three modes to cross or take the same frequency as, for instance, for GdCrO$_3$, where only a single intense band is observed around 475 cm^{-1}. Due to the closeness and intercrossing of the three bands, a band assignment of the individual shoulders is only possible on the basis of polarized Raman data on single crystals (available in the literature for some rare earth elements[22,24,35,36]) and on the hypothesis that the A_g mode remains throughout the series the most intense among the three modes. Based on this, we observe that the B_{2g} mode shows the most pronounced low wave number shift and even crosses the two other modes from the high wave number side in LuCrO$_3$ to the low wave number side of the three-mode feature in LaCrO$_3$.

The broadness of the massif at around 580 cm^{-1} suggests two or three underlying bands for this feature, which can unfortunately not be distinguished by our powder Raman experiment, although we note that their presence is suggested by single-crystal data in the literature.[22,24,35,36] Modes in this region involve mainly stretching vibrations of the CrO$_6$ octahedra, which in turn explains their insensitivity to the orthorhombic distortion, similar to observations for equivalent modes in manganites.[26]

5. The particular case of LaCrO$_3$, PrCrO$_3$, and SmCrO$_3$

Figure 2 and the discussion in the previous sections show that the Raman spectra of LaCrO$_3$, PrCrO$_3$, and SmCrO$_3$ present in the low wave number region a spectral signature that is significantly different from the other RCrO$_3$. This difference, which is in agreement with the reduced distortion of these materials when compared to the other rare earth elements (see Fig. 1 and Table I), complicates the assignment of the individual modes, as the spectral changes are no longer smooth. Figure 5 presents a zoom into the 100 to 450 cm^{-1} region for LaCrO$_3$, PrCrO$_3$, and SmCrO$_3$, which illustrates that the assignment of the 300 to 400 cm^{-1} region is still straightforward. However, the region below 300 cm^{-1} is more complex with two A_g modes and two B_{2g} modes and where modes of the same symmetry are likely to interact and mix.

We first discuss the behavior of the B_{2g} modes. It is tempting to relate the lower B_{2g} modes to one type of vibrational mode and the higher-lying B_{2g} to a second mode. However, Fig. 5 shows that the lower B_{2g} mode in LaCrO$_3$ is weak, which is in contrast to its intense and sharp profile throughout the whole series of RCrO$_3$ (including SmCrO$_3$) and the higher B_{2g} mode of LaCrO$_3$. This observation suggests a transfer of intensity which is the classic behavior for mixing of modes of the same symmetry and which are close in wave number, resulting in transfer of their vibrational character. To support

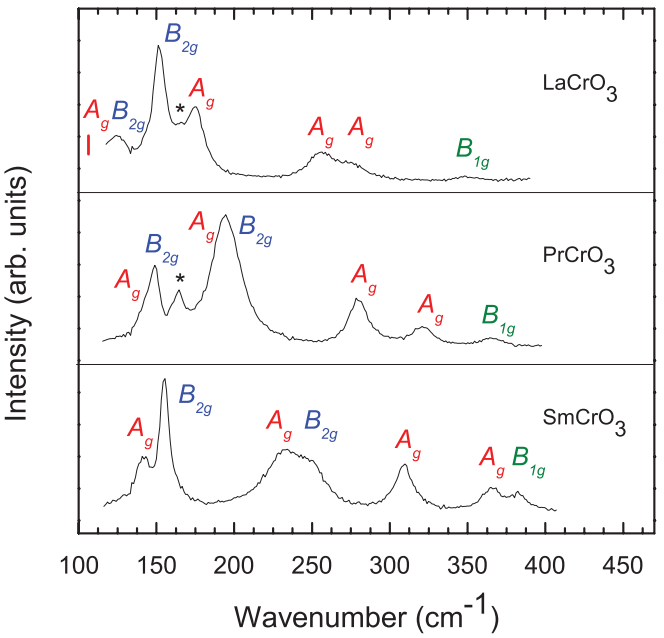

FIG. 5. (Color online) Detailed view and assignment of the Raman modes in the low wave number and mid wave number regions for LaCrO$_3$, PrCrO$_3$, and SmCrO$_3$. The band at 160 cm^{-1}, marked with an asterisk is a spurious line, likely related to an impurity phase. The assignment of LaCrO$_3$, specifically the position and assignment of the 104-cm^{-1} A_g band marked by a red/dark gray line, is from Ref. 22.

this scenario, we consider the mode assignments of lattice-dynamic calculations (LDC) reported for $LaCrO_3$ (Ref. 22) and $YCrO_3$ (Ref. 24), which lead to the following scenario. For all $RCrO_3$ (except $LaCrO_3$ and $PrCrO_3$), the higher B_{2g} (2) mode is activated by the A-cation shift,[24] while the lower B_{2g} (1) mode is activated by octahedral rotations around [101]. For $PrCrO_3$, we expect that the two modes mix and transfer energy, although the overlap of the modes inhibits a detailed analysis. Finally, for $LaCrO_3$, the modes have clearly exchanged their character, as evidenced by the intensity transfer, but our data do not allow judging to what extent the modes are still partly mixed. As a consequence, we assign the 124 cm^{-1} mode in $LaCrO_3$ to B_{2g} (2) and the 154 cm^{-1} mode to B_{2g} (1).

The discussion of the A_g modes on the basis of our own measurements is more difficult as their difference in terms of intensity is less marked and namely because our spectral cutoff does not allow us the observation of the low-lying A_g mode of $LaCrO_3$, which was reported to be located at 104 cm^{-1}.[22] Our discussion thus has to rely on the mode assignments of lattice-dynamic calculations (LDC) reported for $LaCrO_3$ (Ref. 22) and $YCrO_3$ (Ref. 24). According to Ref. 24, the higher A_g (3) mode of $RCrO_3$ (except $LaCrO_3$ and $PrCrO_3$) has the pattern of octahedra rotation, while the lower A_g (2) is dominated by A-cation vibrations. From our data with overlapping modes, it is difficult to judge if the two modes mix for $PrCrO_3$. However, according to the assignment presented in Ref. 22, the two modes have clearly exchanged their character for $LaCrO_3$ so that we assign the 104 cm^{-1} mode in $LaCrO_3$ to A_g (3) and the 175 cm^{-1} mode to A_g (2).

As a consequence, the low wave number region of $LaCrO_3$, $PrCrO_3$, and $SmCrO_3$ is characterized by a complex crossing in between two A_g modes and in between two B_{2g} modes. Further understanding of the mode mixing could be gained from investigations of solid solutions, such as $La_{1-x}Pr_xCrO_3$ or $La_{1-x}Sm_xCrO_3$.

B. Phonon Raman modes vs ionic radii and structural distortions

Figure 6 presents the evolution of the band position for the different chromites as a function of the rare earth R^{3+} ionic radii. The proposed assignment in terms of symmetry and mode crossing is based on the above discussion of the individual spectral regions. The figure illustrates the overall trend of decreasing band positions with increasing r_R, which naturally correlates with the increase of most bond lengths. The few exceptions to this general trend have been discussed in the previous section.

It can be seen that the r_R-dependent shift in wave number varies significantly among the different Raman modes, and it is natural to expect that the modes with a significant shift involve O-Cr-O bending (thus octahedra tilting), as this is the main structural distortion that changes throughout the series. Before discussing this in more detail, we shall recall early work by Scott *et al.*[16,17,19] which demonstrated that Raman spectroscopy allows investigating the distortion of perovskites that is caused by the rotation of octahedra. By studying temperature-dependent Raman spectra of $SrTiO_3$ (Ref. 16) and $LaAlO_3$ (Ref. 17) across their phase transition from a noncubic structure with octahedra tilts to the undistorted

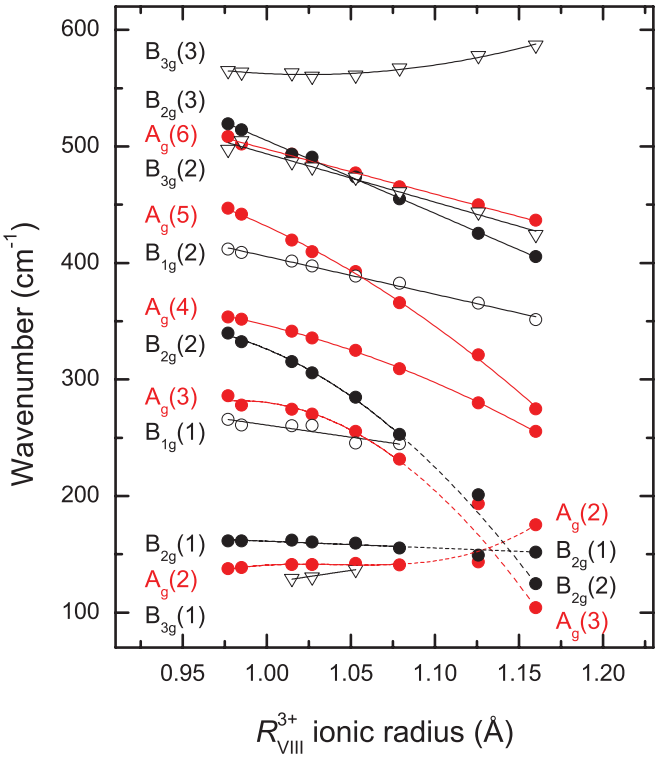

FIG. 6. (Color online) Raman phonon wave numbers of $RCrO_3$ as a function of the rare earth R^{3+} ionic radius. All lines are guides to the eye only. The dashed lines for the low wave number modes indicate schematically the region of mode mixing, discussed in the text.

cubic structure, they have observed that the phase transition is driven by soft modes which scale with the angle of rotation of the octahedra. This Raman soft-mode picture has later described also the behavior of the same model materials under high pressure.[20,23,48,49] As this soft mode concept is of importance for the interpretation of our data, we will shortly illustrate its application to the relatively simple model system $LaAlO_3$ (LAO). Here, LAO crystallizes in a rhombohedral R-3c structure that is characterized by an antiphase $a^-a^-a^-$ tilt of the adjacent AlO_6 octahedra about the $[111]_p$ pseudocubic diagonal, which gives rise to five Raman-active modes $\Gamma_{\text{Raman}} = A_{1g} + 4E_g$. The A_{1g} and one E_g mode of the rhombohedral structure are mainly related to the collective modes of the octahedral network. The vibration of the A_{1g} mode specifically has the pattern of the single rotation of adjacent AlO_6 about the [111] axis.[17,27,50,51] Experimentally, the position of the A_{1g} modes shows a linear scaling behavior with the AlO_6 octahedral rotation angle with a slope of about 23.5 $cm^{-1}/^{\circ}$.[50,51] Here, $LaNiO_3$, which adopts the same structure but has a different chemistry, presents interestingly a similar slope of 23 $cm^{-1}/^{\circ}$.[47,52] The observed linear relationship is in agreement with Landau theory, which predicts for the simplest second-order phase transition that the soft-mode frequency ω should vary in the distorted phase ($T < T_c$) with temperature as $\omega^2 = A(T_c - T) \sim \theta^2$, where θ is the octahedral rotational order parameter.[53]

The situation is more complicated in perovskites with a *Pnma* structure, because several soft modes take part in the

lattice distortion. The structure can either be described in terms of three orthogonal tilt angles (leading to the $a^-b^+a^-$ Glazer's notation) or by rotations θ, ϕ, and Φ around the pseudocubic $[101]_{pc}$, $[010]_{pc}$, and $[111]_{pc}$ axes, respectively.[1] Under the assumption that the orthogonal rotations $a^-{}_x$ and $a^-{}_z$ are approximately equal in the *Pnma* structure, it has been shown by Megaw[54] that the tilt angles θ and ϕ alone are sufficient for describing the octahedral tilting of the structure, while the angle Φ can be obtained via $\cos\Phi = \cos\theta\cos\phi$.[1] The necessary requirement for correlating the two tilt angles θ and ϕ to the observed Raman signature is the knowledge of the distortion-dependent soft modes, for which Iliev *et al.*[26] have shown that they are of A_g symmetry. This identification of this mode is not trivial, given the important number of Raman-active modes in the *Pnma* structure. Also, the *Pnma* structure is among the most stable structures within perovskites, so that usually only a weak softening is observed, complicating the identification of the vibrational modes which present the pattern of the distortion.

In the past, the empirical comparison of several materials with the same type of structural distortion has been used to overcome this problem and has been a rich source of understanding Raman signatures in oxide materials. For the specific case of orthorhombic perovskites, we mention the systematic Raman work on orthorhombic RMnO$_3$ orthomanganites[26,30,31] and RScO$_3$ orthoscandates,[55–57] all of which crystallize in the same *Pnma* symmetry as orthochromites. These studies have allowed identifying two A_g modes with an octahedra-rotation vibrational pattern of which the frequency scales linearly with the rotation angle of the BO_6 octahedral tilting.[26,55] Interestingly the observed slopes, 23.5 cm^{-1}/° for manganites[26] and 20 cm^{-1}/° for scandates,[55] are close to the value observed for rhombohedral perovskites (see above).

We now discuss the observed spectral changes in our orthochromites. The inspection of Fig. 6 shows that the A_g (5) mode presents a particularly pronounced shift in position with increasing r_A; it is thus natural to assign this mode to one of the two A_g octahedral soft modes which are expected to scale with one of the octahedra tilt angles. Figure 7 plots the A_g (5) phonon positions as a function of octahedra tilt angles for those RCrO$_3$ where available atomic coordinates allow a reliable calculation of the octahedra tilt angles (see Tables I and II for explicit values). It can be seen that the positions of the A_g (5) mode in RCrO$_3$ shows the same tendency as the manganite and scandate modes, i.e. they scale linearly with the octahedra tilt angles at a slope of ≈24.3 cm^{-1}/degree, adding further support to the assignment of the A_g (5) mode. The visual assignment of the second soft mode is less straightforward, as no other A_g Raman mode shifts for the small A cations in a similarly strong way as A_g (5). However, the earlier work on manganites and scandates suggests that both A_g soft modes lie on the same slope (see Refs. 26 and 55 and Fig. 7). As a consequence of this, we have plotted the evolution of all A_g modes against the second tilt mode by assuming the 24.3 cm^{-1}/° slope observed for A_g (5). This plot (not shown) illustrates that only the evolution of the A_g (3) mode follows the behavior of the A_g (5), allowing assigning the A_g (3) mode as the second soft mode, in agreement with earlier assignments of LaCrO$_3$ (Ref. 22) and YCrO$_3$ (Ref. 24). As a matter of fact, this identification has also provided confidence to our assignment of the low-frequency region (see Sec. III A 5).

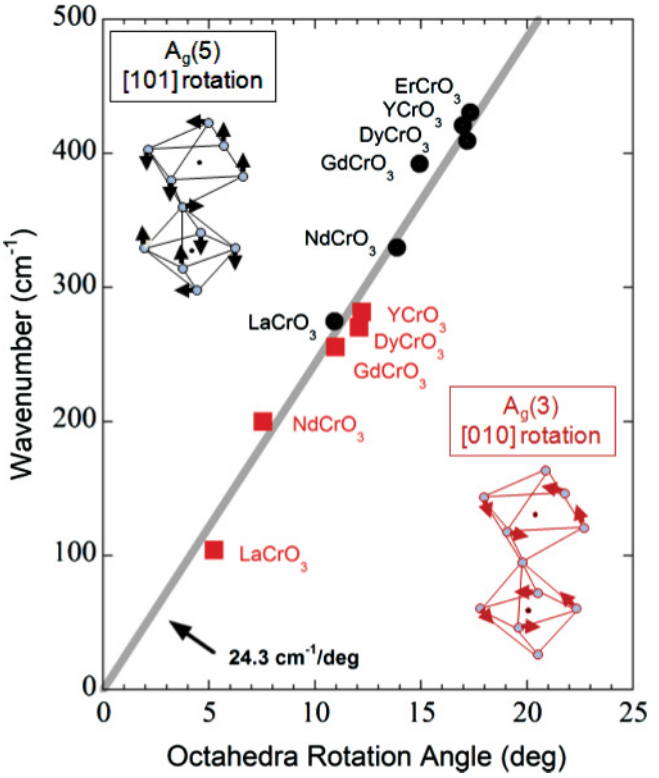

FIG. 7. (Color online) Phonon wave numbers as a function of octahedra tilt angles for A_g (3) [red/dark gray squares] and A_g (5) [black circles] modes of those RCrO$_3$ for which the tilt angle can be calculated from available atomic positions. Raman band positions for NdCrO$_3$ (Ref. 38) and ErCrO$_3$ (Ref. 37) are from the literature.

On the basis of these findings, we conclude that the A_g (5) soft mode is an excellent signature for determining the magnitude of the octahedral rotation in orthorhombic RCrO$_3$ and thus for its deviation from the cubic structure. The A_g (5) is preferred to the A_g (3) on the basis of its easy identification throughout the whole series and because the A_g (3) mode is for large r_R likely affected by mode repulsion and intermixing with the A_g (2) mode, as discussed in Sec. III A 5. This observation in orthochromites, thus in a further family to orthomanganite and orthoscandate perovskites, adds further support to the earlier proposition[26,55] that a general relationship between the angle of octahedral tilting and the frequency of the rotational soft modes is viable in a vast number of perovskites and thus suggests a general soft-mode type relation of the type $\omega^2 = B(r_{R,c} - r_R) \sim \theta^2$, where B is a scaling constant, r_R is the ionic radius of the rare earth, and $r_{R,c}$ the hypothetical ionic radius for which the octahedra tilt becomes zero.

IV. CONCLUSION

We have presented a Raman scattering investigation of a series of nine RCrO$_3$ (R = Y, La, Pr, Sm, Gd, Dy, Ho,Yb, and Lu) powder samples. A symmetry assignment of the observed modes has been proposed on the basis of earlier published single-crystal data for some orthochromites and by taking advantage of the continuous changes in the Raman spectra

across the whole $R\mathrm{CrO}_3$ series. This careful assignment has allowed verifying the reported literature assignments, assigning the modes for the not-yet-reported samples, investigating the complex crossing of several modes and, in particular, relating several modes to the structural distortion of the orthochromites. We have shown that the frequency of the A_g (5) correlates in a soft mode fashion with the magnitude of the octahedral rotation in $R\mathrm{CrO}_3$ and can thus be used to follow the distortion of the structure.

The room-temperature Raman spectra and the associated phonon mode assignment provide reference data for structural investigation of the whole series of $R\mathrm{CrO}_3$ chromites, including the investigation of strain (via phonon shifts) in thin films. Similarly to previous systematic work on manganites,[25] it will be interesting to investigate the A-cation-dependent spin-phonon coupling in orthochromites via Raman scattering through the magnetic phase transition. We also note that recent *ab-initio* calculations of phonon properties have shown to be a great source of understanding for structural and physical properties of perovskite-type oxides. Our study provides benchmark data for such calculations on orthochromites, similar to recent work in the field.[52,58,59]

ACKNOWLEDGMENTS

J.K. is grateful for a visiting fellowship from the Institute of Advanced Study Warwick and acknowledges financial support from the Department of Physics of the University of Warwick during his sabbatical stay at Warwick. Some of the equipment used at the University of Warwick was obtained through the Science City Advanced Materials project "Creating and Characterizing Next-Generation Advanced Materials". O. Chaix, Grenoble, is acknowledged for a careful reading of the manuscript.

*Corresponding author: jens.kreisel@grenoble-inp.fr; Dr. Jens Kreisel, Lab. Materiaux et Genie Physique, MINATEC—Grenoble INP, 3, parvis Louis Neel, 38016 Grenoble Cedex 1, France.

[1] R. H. Mitchell, *Perovskites: Modern and Ancient* (Almaz Press, Ontario, 2002), p. 318.
[2] M. Fiebig, J. Phys. D **38**, R123 (2005).
[3] R. Ramesh and N. A. Spaldin, Nat. Mater. **6**, 21 (2007).
[4] J. Kreisel, B. Noheda, and B. Dkhil, Phase Transitions **82**, 633 (2009).
[5] A. M. Glazer, Acta Crystallogr. Sect. A **31**, 756 (1975).
[6] A. M. Glazer, Acta Crystallogr. Sect. B **28**, 3384 (1972).
[7] A. M. Glazer, Phase Transitions **84**, 405 (2011).
[8] E. F. Bertaut, J. Marescha, G. Devries, R. Aleonard, R. Pauthene, J. Rebouill, and V. Zarubick, IEEE Trans. Magn. **MAG2**, 453 (1966).
[9] K. Tsushima, K. Aoyagi, and S. Sugano, J. Appl. Phys. **41**, 1238 (1970).
[10] K. Sardar, M. R. Lees, R. J. Kashtiban, J. Sloan, and R. I. Walton, Chem. Mater. **23**, 48 (2011).
[11] J. R. Sahu, C. R. Serrao, N. Ray, U. V. Waghmare, and C. N. R. Rao, J. Mater. Chem. **17**, 42 (2007).
[12] Y. L. Su, J. C. Zhang, L. Li, Z. J. Feng, B. Z. Li, Y. Zhou, and S. X. Cao, Ferroelectrics **410**, 102 (2010).
[13] A. Durán, A. M. Arévalo-López, E. Castillo-Martínez, M. García-Guaderrama, E. Moran, M. P. Cruz, F. Fernández, and M. A. Alario-Franco, J. Solid State Chem. **183**, 1863 (2010).
[14] C. R. Serrao, A. K. Kundu, S. B. Krupanidhi, U. V. Waghmare, and C. N. R. Rao, Phys. Rev. B **72**, 220101 (2005).
[15] Z. X. Cheng, X. L. Wang, S. X. Dou, H. Kimura, and K. Ozawa, J. Appl. Phys. **107**, 09D905 (2010).
[16] P. A. Fleury, J. F. Scott, and J. M. Worlock, Phys. Rev. Lett. **21**, 16 (1968).
[17] J. F. Scott, Phys. Rev. **183**, 823 (1969).
[18] G. Burns and B. A. Scott, Phys. Rev. B **7**, 3088 (1973).
[19] J. F. Scott, Rev. Mod. Phys. **46**, 83 (1974).
[20] P. Bouvier and J. Kreisel, J. Phys. Condens. Matter **14**, 3981 (2002).
[21] J. Kreisel, P. Jadhav, O. Chaix-Pluchery, M. Varela, N. Dix, F. Sánchez, and J. Fontcuberta, J. Phys. Condens. Matter **23**, 342202 (2011).
[22] M. N. Iliev, A. P. Litvinchuk, V. G. Hadjiev, Y. Q. Wang, J. Cmaidalka, R. L. Meng, Y. Y. Sun, N. Kolev, and M. V. Abrashev, Phys. Rev. B **74**, 214301 (2006).
[23] M. Guennou, P. Bouvier, J. Kreisel, and D. Machon, Phys. Rev. B **81**, 054115 (2010).
[24] N. D. Todorov, M. V. Abrashev, V. G. Ivanov, G. G. Tsutsumanova, V. Marinova, Y. Q. Wang, and M. N. Iliev, Phys. Rev. B **83**, 224303 (2011).
[25] J. Laverdière, S. Jandl, A. A. Mukhin, V. Y. Ivanov, V. G. Ivanov, and M. N. Iliev, Phys. Rev. B **73**, 214301 (2006).
[26] M. N. Iliev, M. V. Abrashev, J. Laverdière, S. Jandl, M. M. Gospodinov, Y. Q. Wang, and Y. Y. Sun, Phys. Rev. B **73**, 064302 (2006).
[27] M. V. Abrashev, A. P. Litvinchuk, M. N. Iliev, R. L. Meng, V. N. Popov, V. G. Ivanov, R. A. Chakalov, and C. Thomsen, Phys. Rev. B **59**, 4146 (1999).
[28] C. Girardot, J. Kreisel, S. Pignard, N. Caillault, and F. Weiss, Phys. Rev. B **78**, 104101 (2008).
[29] M. Zaghrioui, A. Bulou, P. Lacorre, and P. Laffez, Phys. Rev. B **64**, 081102 (2001).
[30] M. N. Iliev, M. V. Abrashev, H. G. Lee, V. N. Popov, Y. Y. Sun, C. Thomsen, R. L. Meng, and C. W. Chu, Phys. Rev. B **57**, 2872 (1998).
[31] M. N. Iliev, M. V. Abrashev, H. G. Lee, V. N. Popov, Y. Y. Sun, C. Thomsen, R. L. Meng, and C. W. Chu, J. Phys. Chem. Solids **59**, 1982 (1998).
[32] R. M. White, R. J. Nemanich, and C. Herring, Phys. Rev. B **25**, 1822 (1982).
[33] S. Venugopalan, M. Dutta, A. K. Ramdas, and J. P. Remeika, Phys. Rev. B **31**, 1490 (1985).
[34] J. Kreisel, G. Lucazeau, and H. Vincent, J. Solid State Chem. **137**, 127 (1998).
[35] M. Udagawa, K. Kohn, N. Koshizuka, T. Tsushima, and K. Tsushima, Solid State Commun. **16**, 779 (1975).
[36] W. Kaczmarek and I. Morke, J. Magn. Magn. Mater. **58**, 91 (1986).

[37]D. Ullrich, R. Courths, and C. Vongrundherr, Physica B & C **89**, 205 (1977).
[38]Y. Du, Z. X. Cheng, X.-L. Wang, and S. X. Dou, J. Appl. Phys. **108**, 093914 (2010).
[39]Y. S. Zhao, D. J. Weidner, J. B. Parise, and D. E. Cox, Phys. Earth Planet. Inter. **76**, 17 (1993).
[40]R. D. Shannon, Acta Crystallogr. A **32**, 751 (1976).
[41]J. Prado-Gonjal, R. Schmidt, D. Ávila, U. Amador, and E. Morán, J. Eur. Ceram. Soc. **32**, 611 (2012).
[42]N. Sakai, H. Fjellvag, and B. C. Hauback, J. Solid State Chem. **121**, 202 (1996).
[43]K. Ramesha, A. Llobet, T. Proffen, C. R. Serrao, and C. N. R. Rao, J. Phys. Condens. Matter **19**, 102202 (2007).
[44]Z. A. Zaitseva and A. L. Litvin, Dopovidi Akademii Nauk Ukrainskoi Rsr Seriya B-Geologichni Khimichni Ta Biologichni Nauki **1**, 27 (1979).
[45]B. Vanlaar and J. B. A. Elemans, J. Phys. **32**, 301 (1971).
[46]J. Kreisel, G. Lucazeau, C. Dubourdieu, M. Rosina, and F. Weiss, J. Phys. Condens. Matter **14**, 5201 (2002).
[47]N. Chaban, M. Weber, J. Kreisel, and S. Pignard, Appl. Phys. Lett. **97**, 031915 (2010).
[48]A. Grzechnik, G. H. Wolf, and P. F. McMillan, J. Raman Spectrosc. **28**, 885 (1997).
[49]M. Guennou, P. Bouvier, G. Garbarino, and J. Kreisel, J. Phys. Condens. Matter **23**, 395401 (2011).
[50]S. A. Hayward, F. D. Morrison, S. A. T. Redfern, E. K. H. Salje, J. F. Scott, K. S. Knight, S. Tarantino, A. M. Glazer, V. Shuvaeva, P. Daniel, M. Zhang, and M. A. Carpenter, Phys. Rev. B **72**, 054110 (2005).
[51]A. Dubroka, J. Humlíček, M. V. Abrashev, Z. V. Popović, F. Sapiña, and A. Cantarero, Phys. Rev. B **73**, 224401 (2006).
[52]G. Gou, I. Grinberg, A. M. Rappe, and J. M. Rondinelli, Phys. Rev. B **84**, 144101 (2011).
[53]E. K. H. Salje, *Phase Transitions in Ferroelastic and Co-elastic Crystals* (Cambridge University Press, Cambridge, 1993), p. 300.
[54]H. D. Megaw, *Crystal Structures: A Working Approach* (Saunders Co, Philadelphia, 1973), p. 563.
[55]O. Chaix-Pluchery and J. Kreisel, Phase Transitions **48**, 542 (2011).
[56]O. Chaix-Pluchery, D. Sauer, and J. Kreisel, J. Phys. Condens. Matter **22**, 165901 (2010).
[57]O. Chaix-Pluchery and J. Kreisel, J. Phys. Condens. Matter **21**, 175901 (2009).
[58]P. Hermet, M. Veithen, and P. Ghosez, J. Phys. Condens. Matter **21**, 215901 (2009).
[59]P. Hermet, M. Goffinet, J. Kreisel, and P. Ghosez, Phys. Rev. B **75**, 220102(R) (2007).